Journal of the European Ceramic Society **11** (1993) 189–199

Effect of Grain Size on Yttrium Grain Boundary Segregation in Fine-grained Alumina

P. Gruffel & C. Carry

Laboratoire de Céramique, Swiss Federal Institute of Technology, CH-1015 Lausanne, Switzerland

(Received 19 March 1992; accepted 18 May 1992)

Abstract

In this work, the effects of the mean grain size and of the total yttrium content on the distribution of this element in fine-grained alumina are studied. The yttrium distribution is determined in the TEM using energy dispersive X-ray analysis by measuring the mean grain boundary composition as well as the mean size and number of precipitates per unit volume. Two different types of microstructure are observed, depending on both the grain size and the total yttrium content: in the first, only grain boundary segregation is observed, whereas in the second, the grain boundaries are saturated with yttrium, resulting in the intergranular precipitation of an yttrium-rich second phase. For a given composition, the microstructure changes from the first kind of microstructure to the second kind during grain growth. Predictions using a simple geometrical model based on the mass conservation of yttrium are in good agreement with the experimental results for both types of microstructure. It is shown that the kinetics of grain growth are not significantly affected by the yttrium when it is used along with magnesia in alumina.

In dieser Arbeit wurden der Einfluß der mittleren Korngröße und des Gesamtgehaltes an Yttrium auf die Verteilung eben dieses Elementes in feinkörnigen Aluminiumoxid-Keramiken untersucht. Die Yttrium-Verteilung wurde mittels energiedispersiver Röntgenanalyse mit dem TEM bestimmt, indem sowohl die mittlere Zusammensetzung der Korngrenzenbereiche, als auch die mittlere Größe und Anzahl der pro Volumen ausgeschiedenen Teilchen gemessen wurde. Zwei verschiedene Gefügetypen können je nach Korngröße und Yttriumgehalt beobachtet werden. Im ersten Fall wird lediglich Korngrenzensegregation festgestellt. Im zweiten Fall dagegen sind die Korngrenzenbereiche hinsichtlich des Yttriumgehaltes gesättigt und es ergibt sich die Ausscheidung einer Yttrium-reichen zweiten Phase in diesen Bereichen. Bei fest vorgegebener Zusammensetzung kann das Gefüge vom ersten Typ infolge von Kornwachstum in ein Gefüge des zweiten Typs übergeführt werden. Vorhersagen aufgrund eines einfachen geometrischen Modells, welches auf der Erhaltung der Bruttokonzentration des Yttriums aufbaut, stehen in guter Übereinstimmung mit den experimentellen Ergebnissen für beide Gefügetypen. Es wird gezeigt, daß die Kinetik des Kornwachstums in Aluminiumoxid-Keramiken nicht sehr stark durch den Zusatz von Yttrium beeinflußt wird, wenn es zusammen mit Magnesiumoxid zugegeben wird.

Dans ce travail, nous étudions les effets de la taille moyenne de grain et du contenu total d'yttrium sur la distribution de cet élèment dans la microstructure d'alumine à grains fins. La répartition de l'yttrium est étudiée en microscopie électronique à transmission qui permet de mesurer la composition moyenne des joints de grain et la taille moyenne et le nombre de précipités par unité de volume. Deux types de microstructure sont observées selon la taille de grain et le contenu en yttrium: dans un cas il s'agit uniquement de ségrégation aux joints de grains alors que dans l'autre les joints de grains sont saturés en yttrium et une précipitation intergranulaire d'une seconde phase riche en yttrium et présente. Pour une composition donnée la microstructure change du premier cas au second pendant la croissance granulaire. Les résultats d'un modèle géométrique simple basé sur la conservation de la masse d'yttrium sont en bon accord avec les observations expérimentales pour les deux types de microstructure. On montre également que la cinétique de croissance granulaire ne varie pas significativement quand on rajoute de l'yttrium à une alumine déjà dopée en magnésie.

Journal of the European Ceramic Society 0955-2219/93/$6.00

1 Introduction

It is well known that grain boundary segregation can strongly affect the macroscopic properties of both metallic and ceramic polycrystalline materials: one of the best known examples is the temper embrittlement of low alloy steels due to antimony grain boundary segregation. Grain boundary segregation, which can be defined as a local variation of composition without the formation of a new phase, has been studied more infrequently in ceramic systems than in metallic ones. In metals, both the elastic field due to the difference in the atomic sizes between the solute and solvent and the mismatch between the crystallographic structures of the two equilibrium phases limit the solubility of the solute in the solvent, i.e. these two factors are responsible for grain boundary segregation. In ceramics, in addition to the elastic strain and the crystallographic mismatch,[1] the different electronic charge associated with each species and space charge effects can also affect the solubility limit and contribute to solute segregation. Two main approaches have generally been applied to treat grain boundary segregation phenomena: thermodynamic, where an analogy with surface adsorption is applied,[2] and atomistic, where the effect of solute addition on the structure of the grain boundary, or the reverse, is investigated by numerical calculations.[3,4] (As in such treatment the positions of the atoms are required, it is clear that it is limited to some grain boundaries.) Recently, a model regrouping these two main approaches has been proposed.[5] Most of the studies concerning grain boundary segregation report the effects of the total solute content and of the temperature. So far, the effect of microstructure has rarely been investigated and, to the authors' knowledge, only the results of Cook & Schrott[6] report the effect of the mean grain size on the segregation of calcium in alumina.

If the solute concentration at the grain boundary is too great, it becomes oversaturated and a new phase is formed. Such a phase transformation occurs by nucleation and growth. These two processes have been widely studied in metals but, in ceramics, the only second phases that have been extensively investigated[7,8] are porosity or cavitation (which may develop during creep) along with the amorphous intergranular phase that is often present due to the impurity content of the raw material.[9] (The cavitation phenomenon is responsible for high-temperature failure and minimizes high-temperature deformation of materials.) In some cases, the newly formed phase can appear as a thin layer at the grain boundaries, which results from a two-dimensional phase transformation.[10] This type of phase transformation, which has been widely reported in metals, affects the structure of the grain boundary.[11]

In the case of Al_2O_3, segregation of many elements has been reported at the free surfaces of monocrystals[12,13] as well as at the grain boundaries in polycrystals.[14,15] In the case of free surfaces, the crystallography of the surface affects segregation and site competition can occur between different segregating elements. For grain boundary segregation, Li & Kingery[14] concluded that it is controlled by an elastic strain effect rather than a charge effect. This conclusion seems valid whether or not the valence state of the solute cations is the same as that of the Al ions (3+). In the case of yttrium in alumina, solute and solvent cations have the same valence state. Consequently, it can be assumed that the strain effect is responsible for segregation and that there is no charge effect and/or modification of the defect concentration when yttrium is added to alumina. In this system, segregation has been reported at the grain boundaries[14,15] and at the free surfaces.[16] For monocrystals, calculations have shown that segregation of yttrium at the free surfaces is related to the crystallography of the surface.[17] Precipitation of yttrium garnet has been reported at the surface of sapphire and the solubility limit of yttrium in the bulk has been evaluated to 10 ppm weight yttrium.[18] In polycrystalline alumina, precipitates of yttrium garnet are formed at the grain boundaries.[16,19] In alumina, doping with yttrium affects properties related to grain boundary phenomena such as diffusion,[19,20] creep,[21,22] grain growth and cavitation occurring during creep.[21-25]

This study reports the effect of the microstructure, which is defined here simply by the mean grain size, on the distribution of yttrium in alumina doped with magnesia and co-doped with yttria using two different concentrations: 500 and 1500 ppm weight. A simple geometrical model [26] based on the mass conservation of yttrium has been applied to explain the variation of mean grain boundary composition with the grain size and the total yttrium content. When observed, the precipitates rich in yttrium are characterized by their mean equivalent diameter and their density per volume unit. The effects of the grain size and of the total yttrium content on the precipitation of the second phase rich in yttrium are reported and discussed. The grain growth kinetics are evaluated for the different materials.

2 Experimental Procedure

Dense fine-grained alumina polycrystals (>99·5%) were obtained by hot-pressing commercially available α-alumina powders (Criceram, Jarrie, France). This operation was performed under vacuum in graphite dies under 45 MPa uniaxial pressure. The

Table 1. Impurity content of the powders given by the supplier (values in ppm weight)

Ca	*Fe*	*Na*	*Si*	*Ga*	*K*[a]
5	9	28	54	7	50

[a] Determined by radio-activation.

different powders were doped by the supplier with 500 ppm weight MgO (referred to as CMG) and co-doped with 500 ppm weight (referred to as CMGY) or 1500 ppm weight Y_2O_3 (referred to as CMG3Y). (MgO is known as a sintering additive in alumina and it has the effect of suppressing abnormal grain growth. The exact mechanism responsible for these effects is still not well understood.) The impurity content of the powders is listed in Table 1. Mean grain sizes were obtained in two different ways: by changing hot-pressing time t and/or temperature T, the latter being held below or equal to 1550°C and by annealing hot-pressed samples in air at 1450°C. Such annealing produces a maximum density loss due to swelling of −0·5%. The mean grain size d ($d = 1{\cdot}38\sqrt{s}$, where s is the grain mean intercept area on a plane section) was measured on scanning electron microscope (SEM) images of polished (using diamond paste) and thermally etched sections. These sections were chosen parallel to the hot-pressing load P. The mean grain size d was evaluated on more than 1000 grains observed in six different positions for each sample. For the different compositions, the grain growth law during annealing at 1450°C was determined from discrete experimental measurements. The grain growth law given by eqn (1) was fitted to these experimental points:

$$d^N - d_0^N = K_N \cdot t \tag{1}$$

In this equation, N is the grain growth exponent, K_N the rate constant [m^N/s], d_0 the initial grain size and t the annealing time.

In order to prepare samples for transmission electron microscopy investigations, disks of 3 mm diameter and 100 μm thick were cut, mechanically dimpled to a thickness of about 30 μm and finally argon ion-thinned at 5 keV. This thin foil was finally carbon coated to avoid charging under the electron beam in the microscope. Grain boundary compositions were determined in a Philips EM430 TEM/STEM (Philips EM430 ST, the Netherlands) using an energy dispersive X-ray detector. All analyses were performed at 300 keV in STEM mode using a probe size D varying between 5 and 10 mm depending on the illumination conditions. For each specimen, the mean grain boundary composition was determined from point analyses performed on ten different grain boundaries; five different point measurements were made along each grain boundary, therefore 50 measurements were made for each sample. X-Rays were collected from 30 to 60 s and converted to composition using the Cliff–Lorimer equation:

$$\frac{C_i}{C_j} = k_{ij}\frac{I_i}{I_j} \tag{2}$$

where C are the concentrations, I the characteristic X-ray intensities of the elements i and j and k_{ij} a constant. The references used in this work are the bulk of a pure alumina for Al and yttria powder (Merck, Zurich, Switzerland) for Y; the quantitative chemical analysis was performed using experimental K factors. Possible effects of the diffraction conditions of one or the two adjoining grain(s) of the analysed grain boundary were neglected.

As in the case of grain boundary analysis the irradiated volume can be larger than the thickness of the solute enriched layer δ, a correction factor has to be applied to the measured grain boundary solute concentration C_{exp} in order to obtain the real grain boundary solute concentration C_{gb}. In the present work, the correction method proposed by Bender *et al.*[15] was used: real grain boundary solute concentration in yttrium, C_{gb}, is then related to the measured one, C_{exp}, by:

$$C_{gb} = C_b + (C_{exp} - C_b)\left(\frac{\pi}{6\delta}\right)\frac{(6D^2 + b^2 + 3bD)}{(4D + b)} \tag{3}$$

where $b = 625(Z/E_0)(\rho/A)^{1/2}t^{3/2}$ (in m), δ is the width of segregated zone, D the probe size (in m), ρ the density ($3{\cdot}986 \times 10^3\,kg\,m^{-3}$), Z the atomic number, E_0 the operating voltage, A the atomic weight, t the local foil thickness (in m) and C_b the solute concentration in the bulk. In the case of alumina, Z and A are considered as the average atomic number and weight respectively ($Z = (3Z_O + 2Z_{Al})/5$). Local foil thickness t was determined for each analysed grain boundary using the convergent electron beam diffraction technique.[27] In this work, C_b was considered as the solubility limit of solute element in sapphire.

All specimens were observed in TEM to check the presence of second phase precipitates. When observed, their composition and crystallographic structure were determined by EDS analysis and electron diffraction, respectively. The yttrium-rich precipitates were located by X-ray mapping using the yttrium L_α characteristic X-ray line ($\approx$15 keV) and the particulate absorption contrast due to the presence of yttrium; their mean size was determined by measuring at least 30 of them. For some samples, the number of precipitates observed in a unit of projected area of the thin foil N_{pr} was determined in TEM. However, as the thickness of the foil is not constant for all the examined area, the volume observed is not known with a good precision and

therefore, N_{pr} cannot be interpreted as a density of precipitates per unit volume N_V without certain assumptions. Another method using dedicated μ-probe was applied to evaluate the volume density of precipitates, but as the limit of detection of this equipment is of about 1 μm, not all precipitates were detected. Indeed, for some samples, no precipitate was detected using the μ-probe even if they were observed in the TEM.

3 Results

Figure 1 shows a lattice fringe imaging of a grain boundary in one of the samples: no amorphous or crystalline intergranular phase can be observed and it is presented here only for the sake of illustration. It is clear that the absence of a glassy intergranular phase in the ceramic cannot be proven by one high-resolution image, because it has been shown, for example, in SiAlON ceramics that not all grain boundaries may contain amorphous phases.[28] Other electron microscopy techniques such as dark-field imaging of diffuse scatter and through focal imaging of fresnel fringes[9] do not show any glassy phase at grain boundaries or triple points in these materials. These aluminas can be considered as polycrystals without any amorphous intergranular phase. On a larger scale, some β'''-Al_2O_3 precipitates rich in potassium are observed in all samples but in a concentration smaller than that reported by Fridez[29] during his examination of alumina containing three times more potassium than was present in the samples investigated in this study.

Typical SEM micrographs of yttria containing samples obtained either by hot-pressing or by hot-pressing followed by annealing are shown in Fig. 2. Neither a high hot-pressing temperature nor a prolonged annealing time could induce abnormal grain growth or a drastic modification of the morphological texture. The grains were consistently observed to be equiaxed from the grain aspect ratio values and no tabular grains were found.

When the probe, which is the incident electron beam in scanning transmission electron microscopy, is fixed in position over the trace of a grain

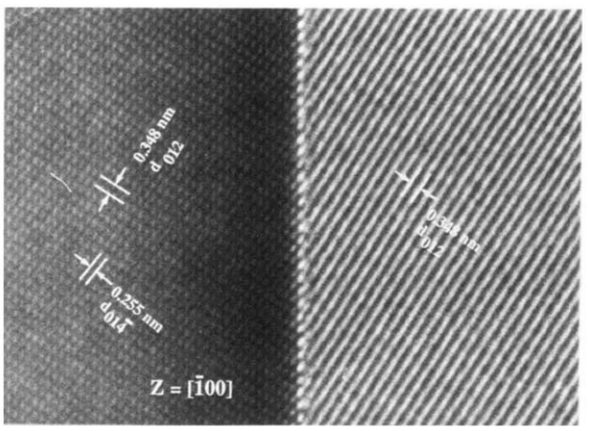

Fig. 1. Lattice fringe imaging of a grain boundary of the aluminas. Crystallographic information is also given for both adjoining grains.

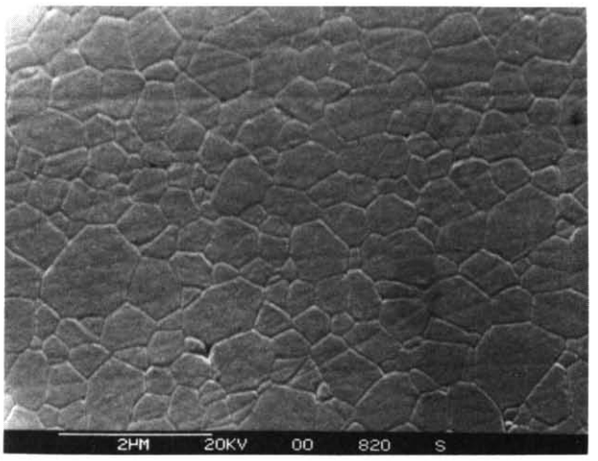

(a)

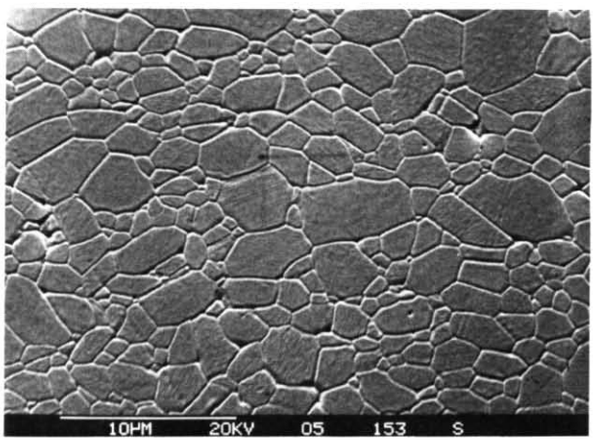

(b)

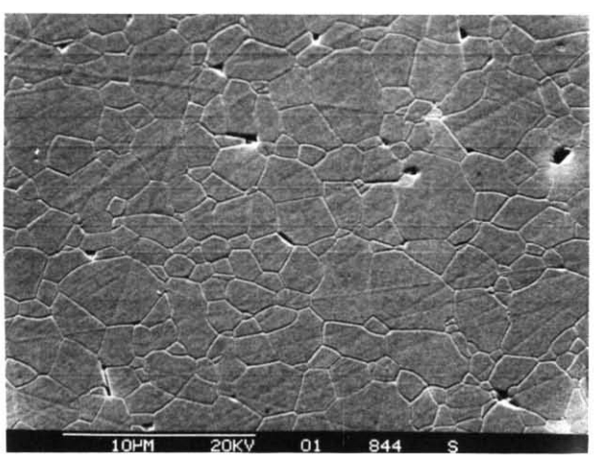

(c)

Fig. 2. Microstructure of fine- and coarse-grained hot-pressed and annealed alumina, SEM micrographs. (a) 1450°C, 15 min, CMGY, $d = 0{\cdot}65\ \mu$m; (b) 1550°C, 75 min, CMGY, $d = 2{\cdot}4\ \mu$m; and (c) 1450°C, 30 min, CMG3Y + annealed in air, 1450°C, 640 min, $d = 2{\cdot}2\ \mu$m.

boundary, an EDS spectrum is obtained which shows the presence of Al and Y. If the probe is moved further than 10 nm from the grain boundary trace, no yttrium is detected. As the thickness of the yttrium-enriched layer δ is approximately the size of the probe diameter D, it is not possible to determine the concentration profile of yttrium at the grain boundary and, in addition, the electron beam spreads due to interactions between the electron beam and the sample.[30] For each point analysis, Al K_α and Y K_α characteristic lines are used to determine experimental composition of the grain boundary C_{exp} from the measured spectrum by applying eqn (3). As the solubility limit of yttrium in sapphire is very low ($\approx$10 ppm weight yttrium),[18] the bulk content in yttrium C_b can be neglected in this equation and $C_{gb}\delta$ can be calculated from the measured yttrium concentration C_{exp} if the probe diameter D (given by the microscope manufacturer for the different conditions of illumination) and the local foil thickness t are known. For a given sample, it is observed that $C_{gb}\delta$ remains almost constant along the same grain boundary but changes from one grain boundary to another. Measurements made on the same sample over a period of several months are reproducible. Figure 3 shows the evolution of $C_{gb}\delta$ with the mean grain size d for CMGY and CMG3Y. For each sample, the bar represents the standard deviation of the composition distribution measured on the different grain boundaries. Assuming that the thickness of the enriched layer δ is independent of the grain size and is the same for both compositions, Fig. 3 shows the evolution of the mean grain boundary composition, C_{gb}, with the mean grain size, d. For CMGY, two different regimes are observed: for grain sizes smaller than 2·3 μm, $C_{gb}\delta$ increases linearly with the grain size and for coarser microstructures, $C_{gb}\delta$ is approximately constant at 20% weight nm. In the case of CMG3Y, grain boundary composition

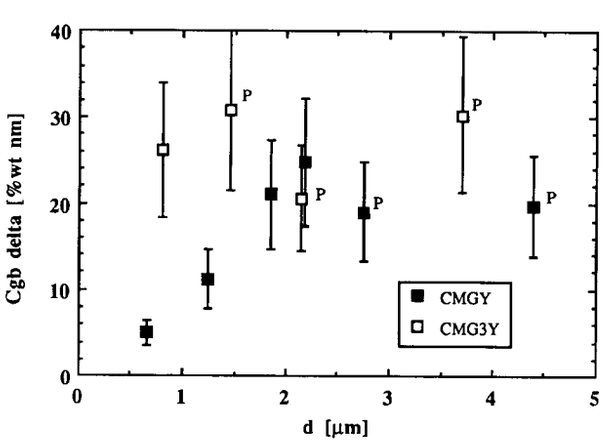

Fig. 3. Evolution of the mean grain boundary content in yttrium $C_{gb}\delta$ with the mean grain size d for yttrium-containing aluminas. Yttrio-garnet precipitates are observed in samples marked with P.

remains almost independent of grain sizes from 0·8 μm (the finest grain size studied for this composition) to 3·4 μm and is approximately 25% weight nm. These results suggest that the grain boundaries become saturated in yttrium as grain growth proceeds and that the saturation composition is independent of the total yttrium content. The grain size at which grain boundaries can be considered saturated decreases with total content in yttrium. In addition, for a grain size of 0·8 μm, C_{gb} is 3·5 times higher in CMG3Y than in CMGY, the ratio corresponding to that of the total yttrium content of these two materials.

In CMGY and CMG3Y, precipitates, in which only yttrium and aluminium are detected by EDS analysis, are observed, provided that the samples have a grain size larger than 2·5 and 1·2 μm respectively (these ones are marked P in Fig. 3). Figure 4 shows bright-field images of such precipitates with the corresponding EDS spectrum and electron diffraction pattern. As illustrated in this figure, precipitates are observed at grain edges, grain corners or along the grain boundaries. Their shapes are more rounded than the alumina grains and small precipitates are observed which have the equilibrium shape (for example lenticular along the grain boundaries). From their composition and crystallographic structure, these precipitates are identified as cubic yttrio-garnet ($3Y_2O_3.5Al_2O_3$) which is the equilibrium phase of alumina oversaturated with yttria at temperatures lower than 1760°C.[31]

Figure 5 shows the evolution of the mean precipitate size, a, with the mean grain size, d, for the two aluminas containing yttrium. The reported curves are calculated using the assumption that the precipitates are spherical (see eqn (8)) and this will also be assumed during the rest of the discussion. For CMG3Y, it can be seen that the precipitate size increases with d. The number of precipitates in a given projected area of the thin foil, N_{pr}, is evaluated at $3{\cdot}5 \times 10^{-2}/\mu m^2$ for CMG3Y, and this seems to be independent of the grain size in the range studied (between 1·2 and 3·4 μm). For CMGY, N_{pr} is not evaluated but is significantly lower. (The experimental determination of N_{pr} is difficult when it is low because a larger area has to be examined in order to obtain a significant result.)

For the different aluminas containing yttria and no yttria, respectively, Fig. 6 shows the evolution of the mean grain size d during annealing in air at 1450°C. Taking into account the uncertainty inherent in the measurement of grain size, the grain growth law given by eqn (1) remains the same for all compositions and is given by:

$$d^3 - d_0^3 = 3{\cdot}4 \pm 0{\cdot}4\, 10^{-4}\,[\mu m^3/s] \cdot t \qquad (4)$$

This result suggests that yttria co-doping has no

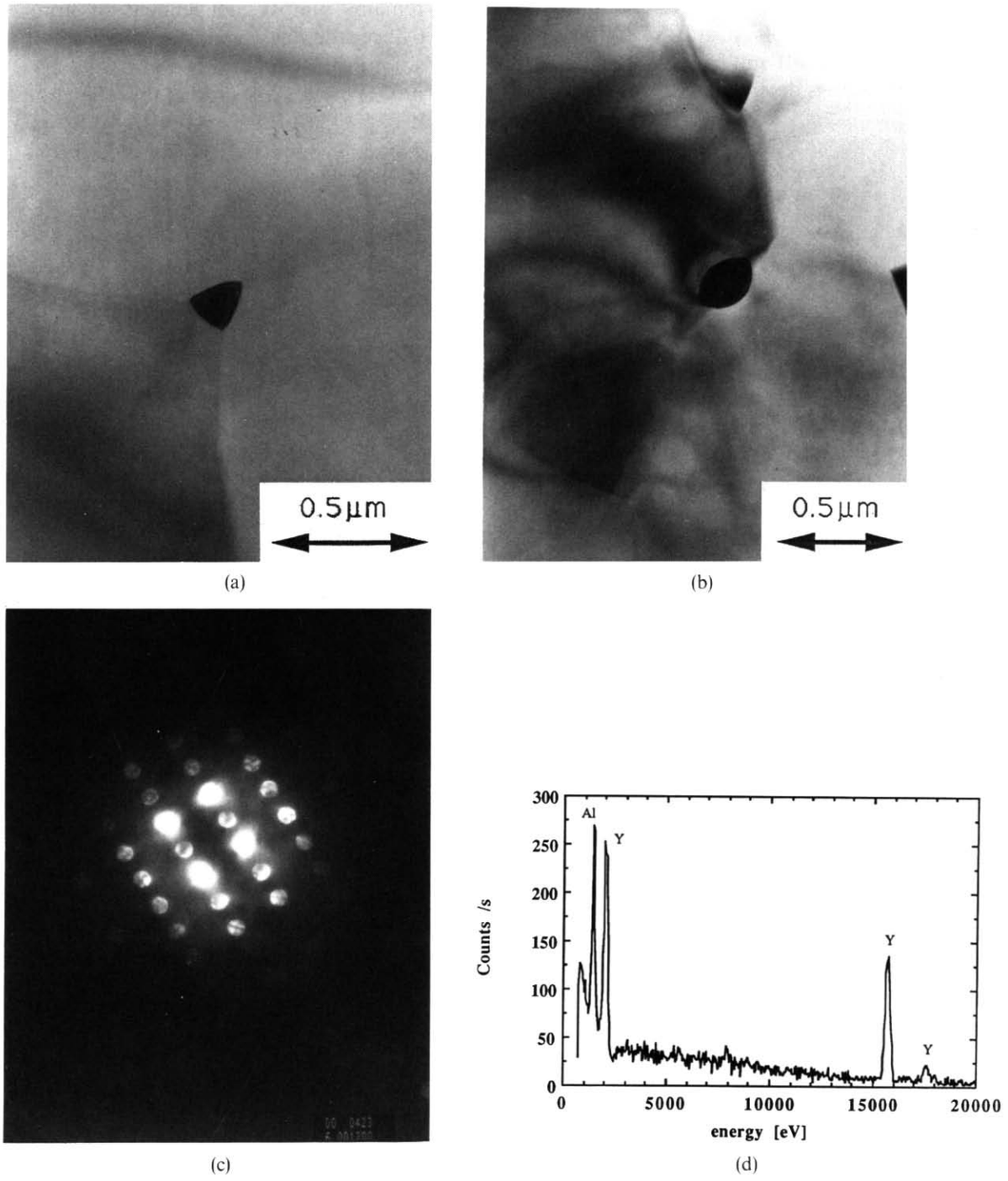

Fig. 4. Yttrio-garnet precipitates: (a) and (b) bright field imaging, (c) corresponding electron diffraction pattern and (d) corresponding EDS spectrum.

significant effect on the grain growth of magnesia-doped alumina under the conditions used during this investigation. Such grain growth as occurs during high-temperature treatments, with or without an applied external stress, can be considered normal from the criterion of the invariability of the normalized diameter distribution, as discussed elsewhere.[32]

4 Discussion

The experimental results are presented in terms of their mean values, although differences in the composition are recorded from one grain boundary to another in the same sample. Such differences have already been reported in ceramics[33] and metals[34] and they have been attributed to an effect caused by the structure of the grain boundary (certain types of grain boundaries, the structures of which are less distorted, contain less solute atoms). This aspect of grain boundary segregation was not studied here and consequently only the mean values of grain boundary composition are presented, discussed and used in the calculations. For the precipitation of yttrio-garnet, which can be considered as a phase transformation by a nucleation–growth process, it is

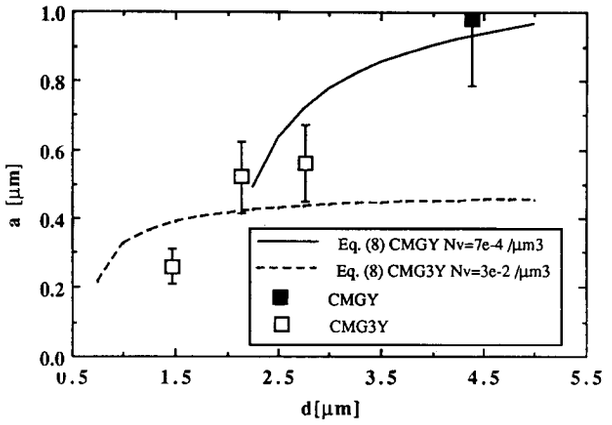

Fig. 5. Evolution of the mean precipitate size a with the mean grain size d for CMGY and CMG3Y. Calculated curves have been obtained from eqn (8) supposing that $C_{gb\,sat}\delta = 23\%$ weight nm (see Fig. 4).

clear that local parameters such as interfacial energies and oversaturation affect the kinetics of both phenomena. In spite of this, as in the case of segregation, only the mean values are considered in the precipitation analysis. These mean assumed values are so similar that each grain boundary and grain can be considered as identical. The principle is frequently applied in the study of polycrystal properties and their relationship with the microstructure.

When treated as a mean value, it has been shown that the grain boundary segregation phenomenon can be affected by both the total content of yttrium and the microstructure (mean grain size d) (Fig. 3). The linear relation between the grain boundary solute content and the total solute content has already been reported in metals[35] and ceramics.[36] In order to quantify the evolution of yttrium distribution during grain growth, a simple model is applied based on the mass conservation of solute element.[26] Its objective is to explain the effect of both the grain size and the total yttrium content on the grain boundary composition. For this purpose, the polycrystal is simplified and is subsequently consi-

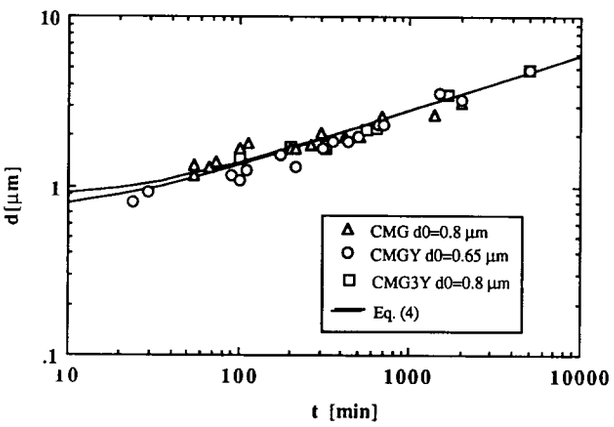

Fig. 6. Evolution of the mean grain size d with annealing time at 1450°C in air for the different compositions. Experimental grain sizes are fitted to eqn (1).

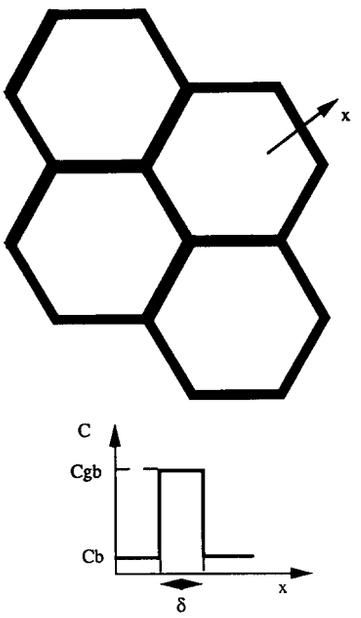

Fig. 7. Schematic representation of the microstructure: two-dimensional idealized case with the concentration profile of yttrium across a grain boundary.

dered as an ensemble of monosized truncated octahedra (this polyhedron has the property of filling the space), each of which is covered with a slice of thickness $\delta/2$ where the concentration of yttrium is constant C_{gb}. Figure 7 shows such a two-dimensional idealized microstructure. When only segregation is observed, the total mass of yttrium is shared between the bulk (in white in Fig. 7) and the enriched zone at the grain boundary (in black in Fig. 7). If the density ρ is independent of the yttrium concentration, the grain boundary concentration C_{gb} is then given by:

$$C_{gb} = \frac{2K_V d}{K_S \delta}(C_{tot} - C_b) + C_b \qquad (5)$$

where C is the concentration in wt%, d the mean grain size and δ the thickness of the enriched layer. The subscripts tot, gb and b refer to total, grain boundary and bulk respectively. K_V and K_S are constants which relate the grain volume and its external surface to its grain size. Details concerning the calculations are given elsewhere.[26] Equation (5), which is an indirect representation of the effect of the volume of a three-dimensional object on the ratio between its external surface and its volume, shows that if the enriched zone thickness δ is constant, C_{gb} increases linearly with d and the total solute content C_{tot}. In addition, it decreases with the solubility limit in the bulk C_b. In the case of yttrium in alumina, as mentioned previously, the solubility limit in sapphire has a value of 10 ppm weight[18] and consequently the second term on the right hand side of eqn (5) can be neglected. The value of $C_{gb}\delta$ can therefore be calculated for different yttrium contents and mean grain sizes d. Calculated curves and experimental

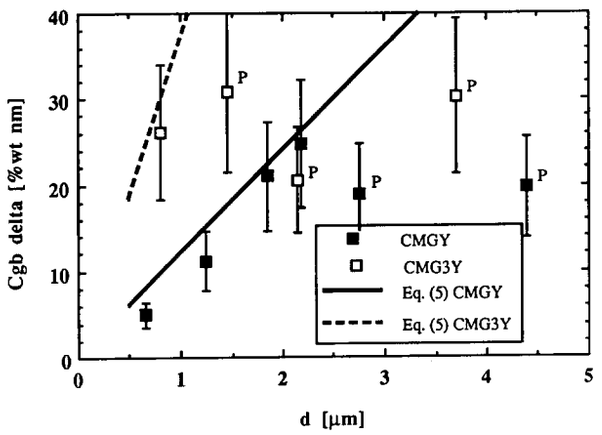

Fig. 8. Evolution of the mean grain boundary solute content $C_{gb}\delta$ with the mean grain size d for yttrium-containing aluminas: both the experimental measurements and calculated curves from eqn (5) are shown.

points are shown on Fig. 8 for CMGY (C_{tot} = 390 ppm weight) and CMG3Y (C_{tot} = 1170 ppm weight). For both these compositions, the calculated curves are in good agreement with the experimental data when the grain sizes are lower than 2·3 and 0·8 μm for CMGY and CMG3Y, respectively. In these ranges, the slight difference between calculated and measured values can be attributed to an underestimation of the probe size D; from eqn (3) that would have the effect of decreasing the measured values of grain boundary composition. An underestimation of the solubility limit C_b could be another interpretation. For this simple treatment of segregation, the thickness of segregated zone δ does not need to be known for both experimental measurements and calculations; this is a considerable advantage because this value cannot easily be measured. The only restriction on δ is that it has to be smaller than the probe size D in order to apply the correction method proposed by Bender *et* al.[15] These results concerning grain boundary segregation are in opposition with the hypothesis of Brook concerning the effect of solute on grain growth:[37] Brook has assumed that the composition inside the grains changed with grain size, which would mean that the solubility limit in the bulk depends on the grain size. In addition, following the present results, a representation such as shown in Fig. 8 of Ref. 14 would not be rigorously correct because the grain size is not specified.

Away from the grain size ranges in which the correlation between observations and calculations is reasonable (see Fig. 8), the grain boundaries are saturated with yttrium and precipitates of yttrio-garnet are observed. The geometrical model that has been proposed for a microstructure with both segregation and intergranular precipitates[26] can therefore be applied. The conservation of the mass of yttrium is always the foundation of the calculation and subscript pr is used for precipitates. In this case, the grain boundary composition is given by:

$$C_{gb}\delta = (C_{tot} - C_b)\frac{2K_V d}{K_S} - \left(C_{pr}\frac{\rho_{pr}}{\rho} - C_{tot}\right)\frac{2V_{pr}}{K_S d^2} + C_b\delta \quad (6)$$

This equation is similar to eqn (5) apart from the second term of the right hand side which is the contribution of the precipitates. In this case, as $C_{pr} \gg C_{tot}$ ($\approx$45% opposed to 0·039 or 0·17 wt% yttrium), the increase in the volume of precipitates induces a decrease of C_{gb}. Neglecting the bulk content term $C_b\delta$ and supposing that $C_{gb}\delta$ is constant, as is observed in samples in which precipitation has occurred due to the grain boundaries saturation, the volume of precipitate can be calculated from eqn (6):

$$V_{pr} = \frac{\left((C_{tot} - C_b)\frac{2dK_V}{K_S} - C_{gb}\delta\right)d^2}{\left(\left(C_{pr}\frac{\rho_{pr}}{\rho} - C_{tot}\right)\frac{2}{K_S}\right)} \quad (7)$$

The volume fraction of precipitate defined as $F_{pr} = V_{pr}/K_V d^3$ is then given by:

$$F_{pr} = \frac{(C_{tot} - C_b)}{C_{pr}\frac{\rho_{pr}}{\rho} - C_{tot}} - \frac{C_{gb}\delta}{2\left(C_{pr}\frac{\rho_{pr}}{\rho} - C_{tot}\right)\frac{K_V d}{K_S}} \quad (8)$$

For a given grain shape, all terms of eqn (8) are known except $C_{gb}\delta$ which is determined experimentally.

If precipitates are assumed to be spherical, then F_{pr} is given by $N_V(4/3)\pi(a/2)^3$ where N_V and a are the density of precipitates per unit volume and the mean diameter of precipitates, respectively. As the density per unit volume is not experimentally evaluated, when a is known, N_V is considered as an adjustable parameter independent of grain size in eqn (8). The curves calculated in this way using the best value of N_V are shown in Fig. 5 for both compositions. The best values of N_V are approximately $3 \times 10^{-2}/\mu m^3$ and $7 \times 10^{-4}/\mu m^3$ for CMG3Y and CMGY, respectively. For CMG3Y, if the thickness of the thin foil is assumed to be constant at a value of 1 μm, the density of precipitates per unit volume which can be calculated from the measured density of precipitates per projected area N_{pr}, is $3{\cdot}5 \times 10^{-2}/\mu m^3$. This value is in good agreement with the best value of N_V obtained by fitting experimental measurements of the mean size of precipitates to eqn (8).

These results suggest that during grain growth, the grain boundary solute content increases due to the diminution of the area of grain boundary per unit volume. If the grain boundary is considered as a separated phase, it has a fixed solubility limit which

is higher than the bulk one. When this limit is reached, grain boundaries are saturated and, if grain growth continues, the yttrium that cannot be incorporated into the grain boundaries forms precipitates instead. It is interesting to note that in this approach, the precipitation is not considered as a phase transformation by nucleation–growth process. That implies that precipitates do not have to satisfy the critical size requirements of nucleation. Following this approach, the yttrium required to allow growth of precipitates is provided by the yttrium that would normally go to the grain boundaries during grain growth, if they were not saturated. For a given total solute content, this amount is controlled by the grain size and consequently the growth rate of precipitates is indirectly controlled by grain growth. In addition, it can be shown that the rate of accumulation of the excess yttrium into the grain boundary depends on the total yttrium content.[26] Considering precipitation as a phase transformation by a process of nucleation–growth, the growth rate of stable precipitates would be controlled by the diffusion of yttrium towards the precipitates through the grain boundaries. In the present case, it can be shown that the rate of accumulation of yttrium into the grain boundaries is slower than the diffusion of yttrium toward the precipitates and thus the rate of accumulation of excess yttrium at the grain boundaries during the grain growth controls the growth kinetic of precipitates. Evolution of the density of precipitates per unit volume, as well as the absence of a marked solute gradient near the precipitates, are consistent with this conclusion. Moreover, as the rate of accumulation of excess yttrium decreases as the total yttrium content decreases, the number of precipitates required to absorb the excess yttrium will also decrease. This can explain the observed difference in the density of precipitates per unit volume between CMGY and CMG3Y.

The present results show that, during grain growth, the microstructure changes from a microstructure with grain boundary segregation to a microstructure with grain boundary segregation and intergranular precipitates. As this change happens when the grain boundaries are saturated with yttrium, the grain size at which it occurs decreases with the total content of yttrium. The formation of yttrio-garnet intergranular precipitates could be preceded by a two-dimensional phase transformation, as suggested by Guttmann.[10] In the present case, for the composition corresponding to the grain boundary saturation, a layer of yttrio-garnet of approximately 0·5 nm would again cover all grain boundaries. This thickness would represent approximately one half of the cell parameter of the cubic yttrio-garnet (1·2 nm) but was not detected using high-resolution electron microscopy. If a phase transformation occurs, then grain boundary properties such as diffusion could strongly change and the macroscopic behaviour of the material could be affected.

Yttrium does not seem to affect the kinetics of grain growth during annealing at 1450°C. This conclusion is valid if either yttrium only segregates to the grain boundaries or if it segregates and forms intergranular precipitates, because the rate of growth was found to be similar in both cases. Recent preliminary results have shown that an alumina doped only with yttrium shows some of the abnormal grain growth that is commonly observed in alumina without magnesia. This suggests that yttrium does not control grain growth in alumina when magnesia is present and as a result it does not seem to be a good doping element for alumina. Baik & White[13] have proposed that the effects of some elements on grain growth in alumina are related to their free surface segregation behaviour. For magnesia, which is known to control grain growth in alumina, segregation is isotropic, whereas for calcium, which causes abnormal grain growth, segregation is anisotropic. The calculations of Mackrodt & Tasker[17] show that the yttrium segregates to the free surface in an anisotropic way. Therefore, its effect on grain growth can be interpreted by analogy with the predicted effect of Ca and Mg. Reviews of the recent results concerning grain growth in alumina[38,39] suggest that this phenomenon is strongly related to the purity of the material and to the magnesia content. Such observations reinforce the fact that yttrium, when added to alumina as a co-doping element with Mg, does not affect grain growth, which is controlled by Mg.

Recent results[22,24] concerning the creep behaviour of such yttria co-doped aluminas in tension as in compression have shown that the 500 ppm weight Y_2O_3 co-doped alumina (referred to here as CMGY) presents a particular creep regime called the strain rate plateau. That plateau can be defined as a given interval of grain size during which the strain rate remains constant. Creep tests on other compositions (1500 and 1000 ppm weight yttria) show that this interval of grain size changes with total yttrium content and a correlation between creep behaviour and the evolution of the mean grain boundary composition suggests that the strain rate plateau occurs in a given interval of mean grain boundary compositions which is located just before grain boundary saturation.[24]

5 Conclusions

In yttrium co-doped aluminas, the distribution of yttrium during grain growth is affected by the grain

size and the total content in yttrium. Consequently, two different kinds of microstructure are observed: a microstructure with grain boundary segregation of yttrium only and a microstructure which shows both grain boundary segregation and intergranular precipitates rich in yttrium. In the former case, the mean grain boundary content in yttrium varies linearly with mean grain size. In the latter situation, the grain boundary composition is independent of the grain size and of the total yttrium content and the precipitates size increases during grain growth. The transition from the first kind of microstructure to the second one occurs once the grain boundaries are saturated with yttrium and thus the grain size at which this occurs decreases with the total content of yttrium. Such a transition suggests that grain boundaries can be considered as a separate phase with a solubility limit higher than that of the bulk. A simple geometrical model founded on the mass conservation of yttrium can explain the experimental results for both kinds of microstructure. Calculations so obtained are in good agreement with experimental observations. On a larger scale, it is shown that yttrium added to alumina in addition to magnesia does not affect grain growth; this phenomenon seems to be mainly controlled by the magnesia.

Acknowledgements

This work has been supported by the Swiss National Fund for Research. The authors would like also to thank Dr Pierre Stadelmann for his help with the transmission electron microscope.

References

1. Yan, M. F., Cannon, R. M. & Bowen, H. K., Space charge, elastic field and dipole contributions to equilibrium solute segregation at interfaces. *J. Appl. Phys.*, **54** (1983) 764–78.
2. Hondros, E. D. & Seah, M. P., The theory of grain boundary segregation in terms of surface adsorption analogues. *Met. Trans. A*, **8A** (1977) 1363–71.
3. Sutton, A. P. & Vitek, V., An atomistic study of tilt grain boundaries with substitutional impurities. *Acta Met.*, **30** (1982) 2011–32.
4. Hashimoto, M., Ishida, Y., Yamamoto, R. & Doyama, M., Atomic studies of grain boundary segregation in Fe–P and Fe–B alloys—I. Atomic structure and stress distribution. *Acta Met.*, **32** (1984) 1–11.
5. Nowoski, T., Joud, J. C. & Biscondi, M., A thermodynamical model of grain boundary segregation for atomistic calculations. *Colloque de Physique, les éditions de physique (F) Colloque C1, Supplément au n° 1*, **51** (1990) 293–8.
6. Cook, R. F. & Schrott, A. G., Calcium segregation to grain boundary in alumina. *Amer. Ceram. Soc.*, **71** (1988) 50–8.
7. Raj, R. & Ashby, M. F., Fracture at elevated temperature. *Acta Met.*, **23** (1975) 653–66.
8. Evans, A. G., Rice, J. R. & Sills, J. P., Suppression of cavity formation in ceramics: propects for superplasticity. *J. Amer. Ceram. Soc.*, **63** (1980) 368–75.
9. Clarke, D. R., On the detection of thin intergranular films by electron microscopy. *Ultramicroscopy*, **4** (1979) 33–44.
10. Guttmann, M., Grain boundary segregation, two-dimensional compound formation and precipitation. *Met. Trans. A*, **8A** (1977) 1383–401.
11. Sickafuss, K. E. & Sass, S. L., Grain boundary structural transformation induced by solute segregation. *Acta Met.*, **35** (1987) 69–79.
12. Baïk, S., Fowler, D. E., Blakely, J. M. & Raj, R., Segregation of Mg to the (0001) surface of doped sapphire. *J. Amer. Ceram. Soc.*, **68** (1985) 281–6.
13. Baïk, S. & White, C. L., Anisotropic calcium segregation to the surface of Al_2O_3. *J. Amer. Ceram. Soc.*, **70** (1987) 682–8.
14. Li, C. W. & Kingery, W. D., Solute segregation at grain boundaries in polycrystalline Al_2O_3. In *Advances in Ceramics*, Vol. 10, ed. W. D. Kingery. Am. Ceram. Soc., Columbus OH, 1985, pp. 368–78.
15. Bender, B., Williams, D. B. & Notis, M. R., Investigation of grain-boundary segregation in ceramic oxides by analytical scanning transmission electron microscopy. *Amer. Ceram. Soc.*, **63** (1980) 542–6.
16. McCune, R. C., Donlon, W. T. & Ku, R. C., Yttrium segregation and YAG precipitation at the surfaces of yttrium-doped α-Al_2O_3. *J. Amer. Ceram. Soc.*, **69** (1986) C196–C199.
17. Mackrodt, W. C. & Tasker, P. W., Segregation isotherms at the surfaces of oxides. *J. Amer. Ceram. Soc.*, **72** (1989) 1576–83.
18. Cawley, J. D. & Halloran, J. W., Dopant distribution in nominally yttrium-doped sapphire. *J. Amer. Ceram. Soc.*, **69** (1986) C195–C196.
19. Lagrange, M. H., Huntz, A. M. & Laval, J. Y., Effect of yttrium on the microstructure and diffusion properties of α-alumina. *Ann. Chim. Fr.*, **12** (1987) 9–21.
20. Nanni, P., Stoddart, C. T. H. & Hondros, E. D., Grain boundary segregation and sintering of alumina. *Mater. Chem.*, **1** (1976) 297–320.
21. Carry, C. & Mocellin, A., Superplasticity of single phase ceramics. *Ceram. Int.*, **13** (1987) 89–98.
22. Gruffel, P. & Carry, C., Strain rate plateau in creep of yttria-doped fine-grained alumina. In *Proceedings of the 11th RISØ International Symposium on Metallurgy and Materials Science Structural Ceramics—Microstructure and Properties*, ed. J. J. Bentzen J. B. Bide-Sorensen, N. Christianson, A. Horsewell & B. Ralph. Riso National Laboratory, Roskilde, 23, Denmark, 1990, pp. 305–11.
23. Gruffel, P., Carry, C. & Mocellin, A., Effect of testing conditions on superplastic creep of alumina doped with Ti and Y. *Sci. Ceram.*, **14** (1988) 587–92.
24. Gruffel, P., Evolutions microstructurales d'alumines a grains fins dopees a l'yttrium et fluage superplastique. PhD Thesis, EPF Lausanne, No. 921, 1991.
25. Robertson, A. G., Wilkinson, D. S. & Caceres, C. H., Creep and creep fracture in hot-pressed alumina. *J. Amer. Ceram. Soc.*, **74** (1991) 915–21.
26. Gruffel, P. & Carry, C., Effect of grain size on grain boundary segregation and precipitation, unpublished.
27. Tanaka, M. & Terauchi, M., In *Convergent-beam electron diffraction*, ed. JEOL Ltd, Tokyo, 196 Japan, 1985, pp. 38–39.
28. Rühle, M., Bishoff, E. & David, O., Structure of grain boundaries in ceramics. *Ultramicroscopy*, **14** (1984) 37–46.
29. Fridez, J. D., Ètude structurale de la déformation superplastique d'une alumine dense à grains fins. PhD Thesis, EPF Lausanne, No. 656, 1986.
30. Williams, D. B. & Roming, A. D., Studies of interfacial segregation in the analytical electron microscope: a brief review. *Ultramicroscopy*, **30** (1989) 38–51.
31. Phase Diagram for Ceramists, Figure 4370, Am. Ceram. Soc., Columbus OH, supplement 1975.

32. Gruffel, P., Righetti, F. & Carry, C., Evolution of grain shape and size during high temperature creep of yttria-doped fine-grained alumina. *J. Mater. Sci.* In press.
33. Roshko, A. & Kingery, W. D., Segregation at special boundaries in MgO. *J. Amer. Ceram. Soc.*, **68** (1985) C331–C333.
34. Briant, R. L., Source of variability in grain boundary segregation. *Acta Met.* **31** (1983) 257–86.
35. Briant, R. L., Grain boundary segregation of antimony and nickel in iron. *Acta Met.*, **35** (1987) 149–53.
36. Kingery, W. D., Segregation phenomena at surfaces and at grain boundaries in oxides and carbides. *Solid State Ionics*, **12** (1984) 299–307.
37. Brook, R. J., The impurity drag effect and grain growth kinetics. *Scripta Met.*, **2** (1968) 375–8.
38. Handwerker, C. A., Morris, P. A. & Coble, R. L., Effects of chemical inhomogeneities on grain growth and microstructure in Al_2O_3. *J. Amer. Ceram. Soc.*, **72** (1989) 130–6.
39. Rödel, J. & Glaeser, A. M., Anisotropy of grain growth in alumina. *J. Amer. Ceram. Soc.*, **73** (1990) 3292–301.